Chem

CellPress

Article

# Evidence of Spiro-OMeTAD De-doping by *tert*-Butylpyridine Additive in Hole-Transporting Layers for Perovskite Solar Cells

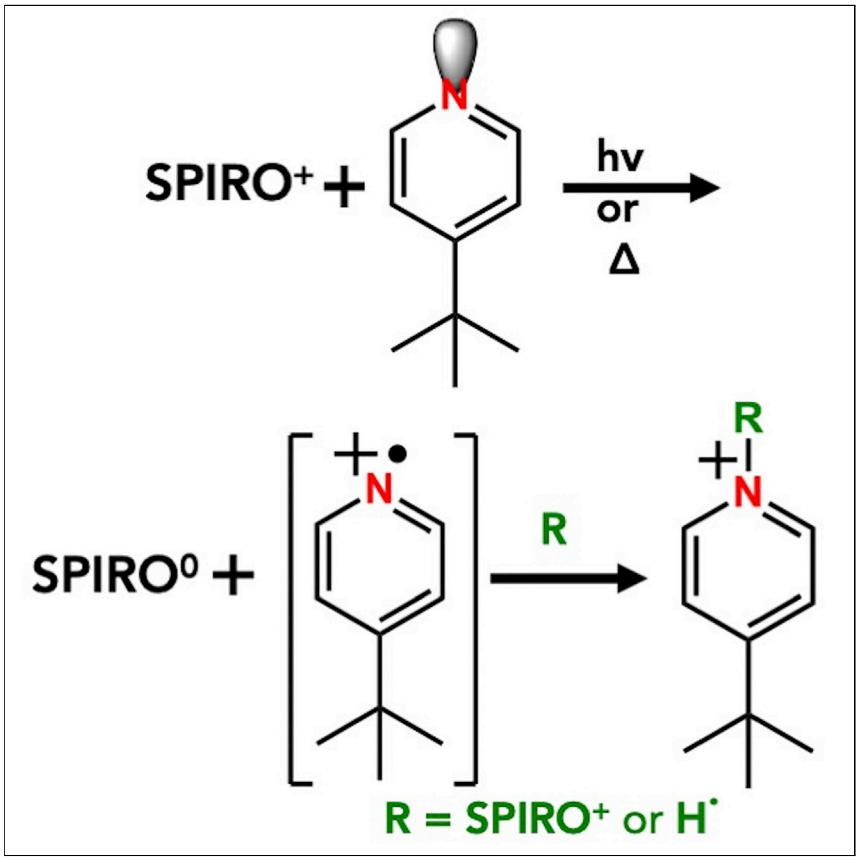


Through a combination of ESR and Raman spectroscopies, a *tert*-butylpyridine-mediated mechanism of Spiro-OMeTAD hole-transporting material de-activation in time is unraveled. The formation of pyridinium salts and neutral Spiro-OMeTAD molecules is the consequence of such a de-doping process.

Francesco Lamberti, Teresa Gatti, Enrico Cescon, ..., Moreno Meneghetti, Annamaria Petrozza, Lorenzo Franco

francesco.lamberti@unipd.it (F.L.)
lorenzo.franco@unipd.it (L.F.)

## HIGHLIGHTS

The de-doping process of Spiro-OMeTAD is detected by ESR spectroscopy

The involvement of the *tert*-butylpyridine additive is demonstrated

A mechanism for this de-activation process is proposed on the basis of Raman evidence

Lamberti et al., Chem 5, 1806–1817
July 11, 2019 
https://doi.org/10.1016/j.chempr.2019.04.003

Chem

CellPress

Article

# Evidence of Spiro-OMeTAD De-doping by *tert*-Butylpyridine Additive in Hole-Transporting Layers for Perovskite Solar Cells

Francesco Lamberti,[1,2,5,*] Teresa Gatti,[1,3] Enrico Cescon,[1] Roberto Sorrentino,[2] Antonio Rizzo,[4] Enzo Menna,[1] Gaudenzio Meneghesso,[4] Moreno Meneghetti,[1] Annamaria Petrozza,[2] and Lorenzo Franco[1,*]

## SUMMARY

**Spiro-OMeTAD is the most-employed molecular hole-transporting material (HTM) in n-i-p perovskite solar cells (PSCs). Ease of processing from solution and good filmability on top of the perovskite photo-active layer are characteristics that make this HTM outstanding and incomparable for the role. However, chemical doping with both *tert*-butylpyridine (tBP) and lithium bis(trifluoromethylsulfonyl)-imide (LiTFSI), coupled with further oxidation steps, is required in order to achieve high hole mobility and conductivity. Previous investigations have revealed that tBP is fundamental for addressing the best morphology in the hole-transporting layer during processing. Here, we provide spectroscopic evidence of the detrimental impact on long-term conservation of Spiro-OMeTAD structural and electrical properties when tBP is used as an additive. These aspects are crucial for the future design and understanding of new molecular HTMs for PSCs.**

## INTRODUCTION

Since the beginning of active research on perovskite solar cells (PSCs), the Spiro-OMeTAD molecule ([2,2′,7,7′-tetrakis(*N*,*N*-di-p-methoxyphenyl-amine)9,9′-spirobifluorene], from now on referred to as SPIRO), has been the most employed hole-transporting material (HTM) in such devices.[1] The main reason relies on the possibility of obtaining the highest figures of merit on as-prepared PSCs because of SPIRO's good wettability on top of the perovskite layer. This property is related to its inherent tridimensional structure, forced by the presence in the central core of the molecule of a SPIRO moiety, as shown in Figure 1A. As a consequence, such a molecular HTM has an excellent pore-filling ability[2,3] coupled with the concomitant ability to provide hole extraction. However, after 6 years of persistent use as a sort of benchmark in PSC development, attempts to substitute it with other HTMs are ongoing[4–7] as a result of several factors that strongly limit the commercialization of PSCs containing it: in particular, the costs of production and the lack of chemical stability that ultimately affects PSC performances after a prolonged time.[8] Furthermore, SPIRO requires an oxidation step for implementation as an HTM:[9] to date, the benchmark process[10] has involved the use of two additives, namely *tert*-butylpyridine (tBP) and lithium bis(trifluoromethylsulfonyl)-imide (LiTFSI) (see Figure 1), in a nitrogen-saturated atmosphere and subsequent overnight storage in a drybox to allow the complete oxidation of the HTM. In order to explain the high hole mobility achieved after proper doping,[11,12] Abate et al., in a seminal work,[13] proposed a two-step mechanism for the formation of Spiro-OMeTAD$^+$

### The Bigger Picture

The development of solid-state hole-transporting materials (HTMs) dates back to the first reports on solid-state dye-sensitized solar cells in 1998, which provided solar cell efficiencies around 1%. The need for these components has then steadily grown with the advent in 2009 of perovskite-based photovoltaics, which cannot sustain any liquid electrolyte. Spiro-OMeTAD molecules have been for many years the material of choice for this application. When doped with LiTFSI salts and *tert*-butylpyridine, the resulting mixture can efficiently extract photogenerated holes in the perovskite absorber and transport them to the collecting electrode. This benchmark for hole transport in third-generation hybrid photovoltaics suffers from intrinsic limitations, which have been studied widely over the years. A detailed molecular-level understanding of the processes involved in Spiro-OMeTAD-based HTM degradation is a key requirement for the future development of new stable and efficient substitutes for this task.

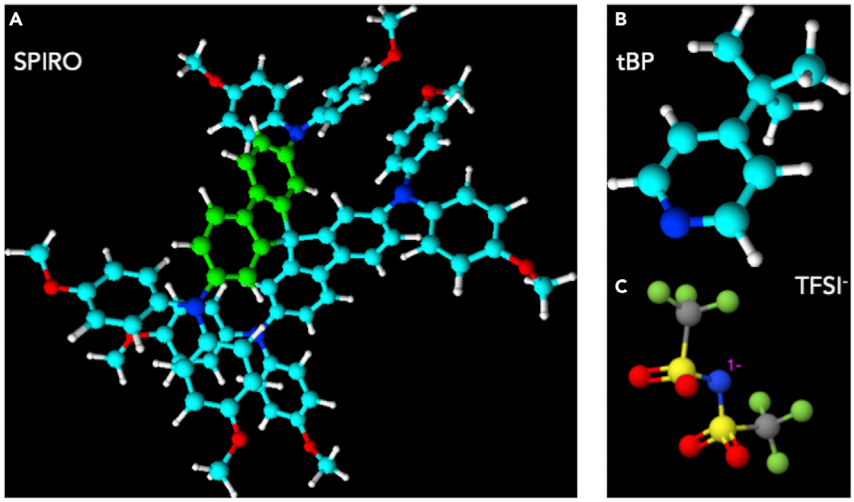


**Figure 1. The Chemicals Used for the Preparation of SPIRO-Based HTMs Depicted in 3D View**
(A) Spiro-OMeTAD (SPIRO): some carbon atoms are painted green to highlight the lack of co-planarity due to the presence of the central spiro moiety.
(B) *tert*-butylpyridine (tBP).
(C) Lithium bis(trifluoromethylsulfonyl)-imide (LiTFSI) (here, the $Li^+$ ion is not displayed).

(hereafter referred to as $SPIRO^+$) from the neutral molecule in the presence of oxygen and LiTFSI:

$$SPIRO + O_2 \overset{h\nu}{\rightleftarrows} SPIRO^{+\bullet}O_2^{\bullet -} \quad \text{(Equation 1)}$$

$$SPIRO^{+\bullet}O_2^{\bullet -} + LiTFSI \overset{h\nu}{\leftrightarrows} SPIRO^{+\bullet}TFSI^- + Li_xO_y, \quad \text{(Equation 2)}$$

in which $Li_xO_y$ represents mixed $Li_2O$ and $Li_2O_2$ oxides produced by $TFSI^-$ anion exchange and reduction of superoxide anion $O_2^-$. The same mechanism was proposed in other studies focusing on $SPIRO^{+\bullet}$ radical formation[11] and investigating the effect of tBP on the HTM morphology[1,14] and solar-cell efficiencies.[15] However, none of the mentioned works paid attention to whether tBP also affects the HTM conductivity (except for a single work highlighting the negative effect of tBP on charge injection efficiency in dye-sensitized solar cells).[16] Indeed, the proposed mechanism considers only the involvement of oxygen and LiTFSI without emphasizing the presence of tBP, which, in standard recipes,[17] is actually used in large excess with respect to the other constituents (about three times more than SPIRO and six times more than LiTFSI). More recently, some interesting works dealing with the interaction between SPIRO and tBP appeared, and they investigated the formation of a pyridinated derivative after light soaking the HTM and the structural modifications (i.e., crystallization versus amorphous state) that can take place when tBP is used in the HTM.[18,19]

Although all these works are very convincing and strengthen the active role of tBP in determining SPIRO behavior in PSCs, none of them directly discuss the structure-property relationships between the solid-state microstructure and the hole-extraction ability of these molecular HTMs, which is the most important information to consider for photovoltaic applications.

For this reason, in this work, we carried out an insightful spectroscopic study on SPIRO-based HTMs used in PSCs to experimentally highlight the detrimental effect of tBP addition that causes a de-doping of the HTM through a mechanism

[1]Department of Chemical Sciences, University of Padova, Via Marzolo 1, 35131 Padova, Italy

[2]Center for Nanoscience and Technology, Italian Institute of Technology, Via Pascoli 70/3, 20133 Milano, Italy

[3]Institute of Physical Chemistry and Center for Materials Research, Justus Liebig University Giessen, Heinrich Buff Ring 17, 35392 Giessen, Germany

[4]Department of Information Engineering, University of Padova, Via Gradenigo 6/a, 35131 Padova, Italy

[5]Lead Contact

*Correspondence:
francesco.lamberti@unipd.it (F.L.),
lorenzo.franco@unipd.it (L.F.)

https://doi.org/10.1016/j.chempr.2019.04.003

consistently linked to the structural changes taking place in the SPIRO molecule after oxidation. It is important to underline how the knowledge of the structural phase of SPIRO molecules in the HTM state can become fundamental for determining the contribution to the overall cell conductivity due to the HTM itself. Recently, Bakr and co-workers experimentally determined the hole mobility of a SPIRO single crystal and found it comparable to that obtained with the oxidized SPIRO molecule in the solid state when used as a thin film within a PSC.[12]

The presence of an unpaired electron in $SPIRO^{+}$ prompted us to employ electron spin resonance (ESR) spectroscopy as a powerful tool for the characterization of this molecular radical with high selectivity and sensitivity, as recently reported.[11,13] We then applied Raman spectroscopy to investigate the structural modifications occurring in time in the prepared HTMs.

## RESULTS AND DISCUSSION

The analytical procedure required the preparation of different tubes for ESR each containing one of four samples. The first sample contained an organic solution of all the three components within the SPIRO-based HTM material, i.e., SPIRO, LiTFSI, and tBP, according to the standard literature procedure.[20] The solvent—a mixture of acetonitrile and dichlorobenzene, as reported in the Experimental Procedures—was then quickly removed under vacuum, and a film was formed on the tube surface (SPIRO:LiTFSI:tBP sample). A second tube was prepared similarly but without tBP (SPIRO:LiTFSI sample). The third one was then prepared without LiTFSI (SPIRO:tBP sample), and the fourth one was prepared with only the pure organic compound (SPIRO sample). The experimental procedure is sketched in Figure 2 for the sake of clarity.

In the dark, SPIRO:LiTFSI provides an intense ESR line originated from a radical species (Figure 3A, green curve). Hereafter, "light-on" and "light-off" indicate that ESR data were collected under light and dark conditions, respectively. The line position (also called g-factor, i.e., the ratio between the spectrometer working frequency and the magnetic field) in the spectrum, although not fully corresponding to the literature value[11] (g = 2.0045 versus 2.0030), is clearly associated with the ESR spectrum of the $SPIRO^{+\bullet}$ radical cation. The slight differences in g-factor values could derive from the different experimental conditions used for the preparation of the films.

The addition of tBP significantly affected the ESR peak intensity and shape (Figure 3A, blue line), as well as any ESR signal that could be found for the control samples (namely, SPIRO and SPIRO:tBP samples) (Figure 3A, red and black lines). In addition, a decrease in time of the $SPIRO^{+\bullet}$ radical signal in the dark was observed for the SPIRO:LiTFSI:tBP sample, as shown in Figure S1, suggesting a time-dependent effect due to interactions among the additives or morphological rearrangements in the solid state. In order to confirm this hypothesis, we performed the same study in liquid (Figure 3B) and found the quenching effect of tBP on a similar ESR signal with faster kinetics than in the solid state as a result of enhanced diffusion. On the other hand, it is peculiar that there was an absence of any change in the line shape of the signal in liquid compared with the solid state: the line shape of the signal from the SPIRO:LiTFSI:tBP solid sample (Figure 3A, blue line) probably reflects the similar line shape found in solution (in the +3.5 h sample in Figure 3B, red curve). However, this signal disappeared in time, and it probably indicates the occurrence of a radical-based process within the sample. Since tBP in the solid state alters not only

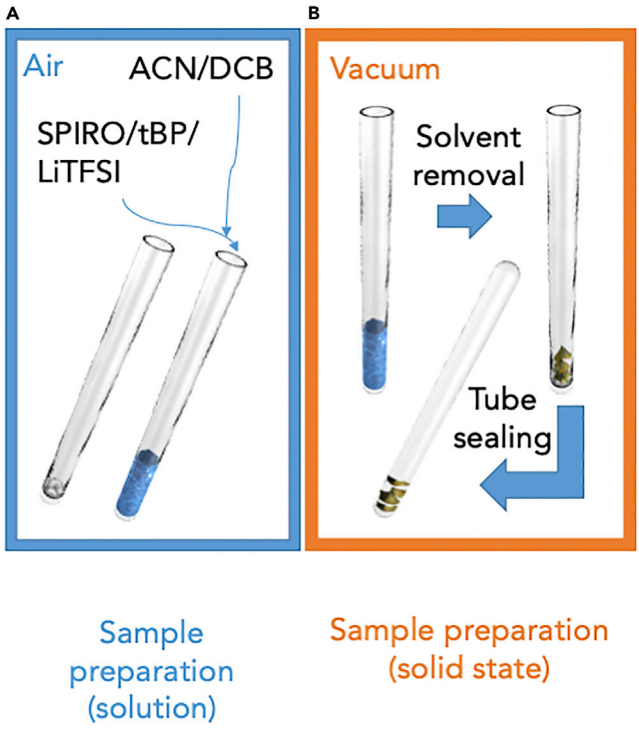


**Figure 2. Experimental Procedure Scheme**

Pictorial sketch depicting the experimental procedure used for the preparation of the two kinds of samples, namely the ones in solution (A) and the ones in the solid state (B), used for ESR characterization.

the intensity of the ESR peak (i.e., the number of spins) but also the line shape (i.e., the structural phase in which the SPIRO molecule is arranged), we carried out a deeper investigation on the interactions occurring between light and the materials in order to gain further insights into the causes of the observed quenching effect.

When the light was switched on, a broad peak (Figure 4A, dark blue line) was generated; the difference between the light-on and light-off ESR spectra is reported in Figure 4A. In addition, by following the evolution of the ESR signal over several days, we observed that a marked change in the shape of the ESR line took place in association with a narrowing of the peak.

We examined the kinetics of light-induced generated radicals and their subsequent decays by considering the time evolution of the ESR spectra after switching the light on or off in a timescale of several minutes. Moreover, we recorded the formation and decay traces on the same sample several days after its preparation. The kinetic traces, reported in Figure 4B, show a continuous change in the ESR signal decay within a period of several days, suggesting an evolution of the solid mixtures, which accelerates the light-induced formation and consequent decay of the $SPIRO^{+\bullet}$ radical. Altogether, these results confirm that the oxidations occurring in the solid state, i.e., the ones that take place during the oxidation step of an HTM within a PSC stored in a drybox, are far from the simple mechanism considered valid up to now (Equations 1 and 2).

The small line width in aggregates is generally due to the fast exchange narrowing normally occurring in highly concentrated radical samples. The high concentration

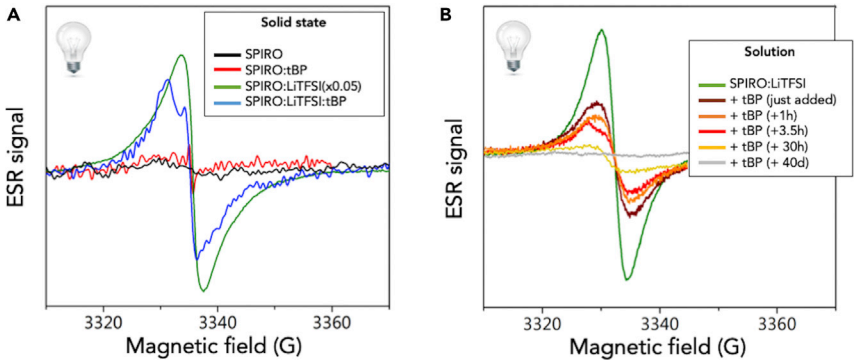


**Figure 3. ESR Characterization**

ESR analysis on the SPIRO molecule after tBP addition in the solid state (A) and acetonitrile dichlorobenzene mixed solution (B).

SPIRO:LiTFSI signal was reduced by a factor of 20 to improve data visualization.

of radicals in the SPIRO:LiTFSI sample evidently produces the observed narrowing of the ESR line. Furthermore, the broader peak is related to several $SPIRO^+$ isolated species. For this reason, the narrow contribution previously found in the ternary HTM SPIRO:LiTFSI:tBP (Figure 3, blue line) ESR spectrum can now be easily attributed to aggregated $SPIRO^+$ domains.

A fast decay is usually related to the presence of a crystalline profile in a semiconductor (i.e., a lower number of traps within the optical band gap), suggesting that an amorphous-to-crystalline transition phase takes place in tBP-rich environments. This hypothesis is supported by Raman analysis of the different sample (Figure 4C). At first sight, indeed, a slight shift toward higher energies of the peak at 732.5 $cm^{-1}$ was found for every sample in which SPIRO aggregates had been detected through ESR. The reagent-grade SPIRO powder—taken as the reference for a crystalline phase—had the highest shift together with the samples containing tBP. This peak is attributed to the $a_1$ fundamental mode of fluorenes[21] (where the two twisted central parts of the SPIRO molecule share a carbon atom), and its shifting toward higher energies (i.e., an increase in the phonon frequency) is due to a compression of the lattice parameters. This evidence further confirms that tBP favors a less amorphous state for SPIRO molecules.

In addition, the peak at 722 $cm^{-1}$ is attributed to the $TFSI^-$ anion coordinated by $SPIRO^+$ species given that the $TFSI^-$ Raman spectrum is known to be affected by ionic coordination[22–24] and is visible only in SPIRO-based samples containing LiTFSI. Moreover, we obtained the reference sample $SPIRO^+TFSI^-$ by simply removing the solvent from the pink solution of SPIRO:LiTFSI, thus allowing us to consider it as the oxidized form of SPIRO, stated as $SPIRO^+TFSI^-$. Nothing can be said of the peaks in the 710–720 $cm^{-1}$ region because of the strong signal of tBP that does not allow a fruitful interpretation of the peaks.

In order to deepen our knowledge of the SPIRO-based HTM and of the effects of additives on carrier life time, we carried out ESR analysis under illumination given that, in this condition, the ESR signals of all samples increased but with different intensities, kinetics, and shapes (Figure S2). In particular, in SPIRO:LiTFSI:tBP, the broader line increased under light irradiation so that the narrower could not be detected, whereas in the other samples, the narrow line was increased by light. The kinetics of formation and decay of the ESR lines are reported in Figure S2. The signal in SPIRO:tBP increased with

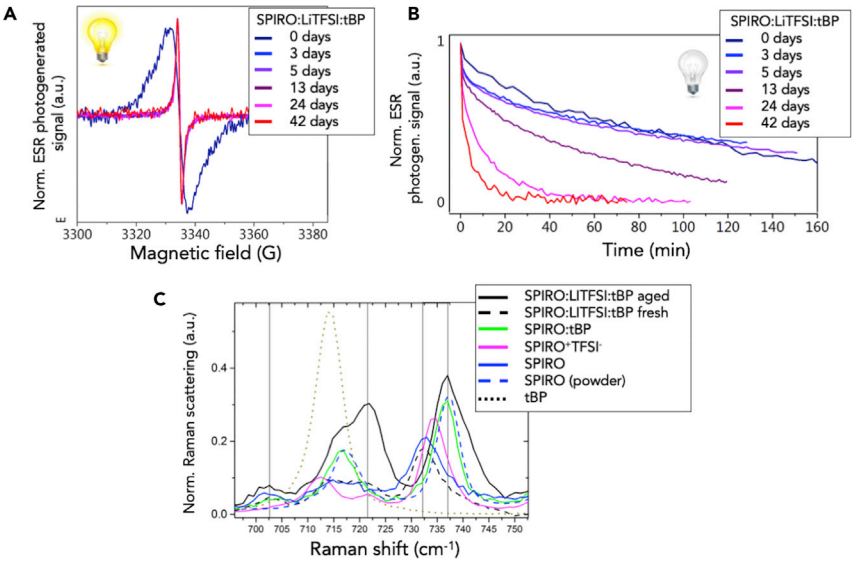


**Figure 4. Physico-Chemical Evidence of the Phase Transition Occurring in the SPIRO Solid Sample**

(A) Light-induced (light-on; light-off) ESR spectra of SPIRO:LiTFSI:tBP in the solid state. Some lines are very similar and therefore impossible to distinguish one from the other.

(B) Time traces of ESR intensity after light-off in SPIRO:LiTFSI:tBP at different days after sample preparation.

(C) Raman analysis of the different SPIRO-based HTMs in the solid state. In particular, "SPIRO (powder)" refers to the reagent-grade SPIRO material taken as a solid, while the reference sample "$SPIRO^{+}TFSI^{-}$" was obtained by removing the solvent *in vacuo* from the solution of SPIRO:LiTFSI.

relatively fast kinetics (a few minutes; Figure S2B), whereas the signal in SPIRO:LiTFSI increased with a much slower rate (several hours; Figure S2B).

The first conclusion to be derived from these data is that, in the dark, tBP inhibits the formation of the $SPIRO^{+}$ species. On the other hand, when the film is continuously irradiated, the tBP-mediated $SPIRO^{+}$ quenching process is not the dominant process, and the oxidation of SPIRO molecules takes place, although less efficiently than in the SPIRO:LiTFSI sample. However, a light-soaking phenomenon (i.e., the formation of persistent $SPIRO^{+}$ species by means of light irradiation) is efficient only in the absence of tBP. The second conclusion is that an oxygen-free oxidation of SPIRO is possible for both SPIRO species (i.e., isolated SPIRO molecules embedded in the film) and aggregated SPIRO.

It is evident that tBP has an active role in determining the electronic properties of SPIRO-based HTMs, but it is not clear whether it is possible to correlate these ESR data to the real processes happening within a PSC. It has been reported that tBP increases the film wettability:[14,25] this evidence is in agreement with the chemical nature of tBP, i.e., a high-boiling-point liquid, and because it is impossible to totally remove it during HTM processing through spin coating on top of the perovskite, it allows the formation of a viscous layer that helps the SPIRO molecules to diffuse. This diffusion then creates some "aggregates of SPIRO molecules" that increase the number of active $SPIRO^{+}$ species. This evidence is corroborated by a study of Juárez-Perez et al.,[1] who showed the formation of segregated domains in doped SPIRO samples (i.e., with the addition of LiTFSI and tBP). Furthermore, we observed that in a SPIRO:LiTFSI sample solution, the flocculation of white particles occurred quickly, as also reported elsewhere.[14] The Raman measurement of the precipitate

unequivocally denoted it as LiTFSI (Figure S3) by the presence of the main peak at 749 $cm^{-1}$ (related to the symmetric deformation of the $-CF_3$ group in the $TFSI^-$ anion).[26] We can therefore state that tBP helps the solubilization of the LiTFSI salt[27] in dichlorobenzene solution, allowing the availability of $TFSI^-$ anion for $SPIRO^+TFSI^-$ species formation.

The aggregated SPIRO signal in the solid state maintains its characteristic behavior (i.e., ESR intensity and slow kinetics) during aging: after 18 days, the amount of photogenerated $SPIRO^+$ species and the rate at which they are formed are unaltered (Figure S4).

The ESR signal of the SPIRO:tBP control sample showed a rearrangement of the materials (Figure S5). After the kinetics of radical formation within the film SPIRO:tBP (Figures S5C and S5D), we detected a little variation of the ESR signal in the dark (Figure S5A), whereas the kinetics remained unchanged after illumination (Figures S5B–S5D). This result confirms that in the solid state, the efficiency of photogeneration is kept constant for the aggregated SPIRO molecules.

At this point, the interpretation of the behavior of the SPIRO:LiTFSI+tBP solid-state sample is straightforward. In the dark (Figures 3A and 3B), $SPIRO^+$ decreased after the addition of tBP. After 40 days, no $SPIRO^+$ was visible any more. More interestingly, the photogenerated ESR spectra (Figure 4A) changed from solvated $SPIRO^+$ (broad ESR line) to aggregated $SPIRO^+$ species (narrow ESR line). The kinetics of quenching of photogenerated $SPIRO^+$ after switching off the light (Figure 4B) were very slow (because of the presence of tBP) in a freshly prepared sample and much faster in an aged sample, similarly to a SPIRO:tBP blend without LiTFSI.

This scenario prompted us to give an overall interpretation of the occurring phenomena in SPIRO-based HTM. The tBP was able to react with the radical $SPIRO^+$.[19] However, because tBP is a high-boiling-point liquid and therefore unremovable from the HTM, in the solid state, it also allows the rearrangement of SPIRO molecules by slowly increasing the crystallinity[12] of the domains of the HTM in its semi-liquid environment. Therefore, among the already recalled morphological and/or solubilizing effects of tBP in SPIRO-based HTMs, this species also has an active role in affecting the overall crystallinity of the film. However, this action is completed in relatively longer times than the other effects.

Soon after the SPIRO film formed in the dark, LiTFSI promoted the generation of $SPIRO^+$ species by electron transfer to molecular oxygen followed by anion exchange and formation of $SPIRO^+TFSI^-$ domains. However, in the presence of tBP, the concentration of SPIRO cation was kept relatively low, as demonstrated by ESR spectra. The effect of light irradiation (light soaking) was to dramatically increase the generation of $SPIRO^+$ species.

More in detail, the chemical role of tBP affects LiTFSI solubility in a chlorobenzene environment by allowing the dissociation of LiTFSI and thus providing solvated $TFSI^-$ ions in solution that may react with $SPIRO^+$, thus producing solid domains of $SPIRO^+TFSI^-$ and lithium mixed oxides (Equation 3):

$$LiTFSI + SPIRO^+O_2^- + tBP \rightarrow Li_xO_y + SPIRO^+TFSI^- + tBP. \quad \text{(Equation 3)}$$

After a while, the morphological role of tBP, affecting SPIRO crystallinity, starts to be relevant in the process. By means of ESR, we were able to distinguish between

amorphous SPIRO and crystalline SPIRO, made by aggregated SPIRO molecules (namely, $SPIRO^{+\bullet}_{(free)}$ and $SPIRO^{+\bullet}_{(agg)}$ species).

In the case of the SPIRO:LiTFSI sample, lacking tBP, the formation of aggregated $SPIRO^{+}$ species in a crystalline phase occurs instantaneously. However, the absence of tBP may alter the solubilization of LiTFSI affecting the availability of $TFSI^{-}$ anion for the formation of highly doped $SPIRO^{+}$ species.

This means that the morphological role of tBP not only is restricted to film wettability during HTM processing but also includes the stable creation of SPIRO aggregates that form an electron-acceptor density-of-states distribution close to the highest occupied molecular orbital (HOMO) band, with a consequent increase in the hole carriers' equivalent mobility.[28] Indeed, the higher mobility in the organic semiconductor used as HTM is obtained by defect-induced doping. Generating electron-acceptor defects in the SPIRO band gap close to the HOMO is equivalent to doping the SPIRO, consequently shifting the Fermi level toward the HOMO band. This situation is achieved only when this defect-induced density of states is very close to the HOMO level of SPIRO molecule, as demonstrated by Fantacci et al.[9]

Therefore, on the one hand, the presence of tBP is required for increasing LiTFSI solubility in dichlorobenzene so that a density of states within the SPIRO band gap is instantaneously generated (i.e., a proper oxidation of SPIRO takes place). On the other hand, tBP acts as a competitor in the time-dependent reaction of $SPIRO^{+}$ species formation by inducing phase segregation inside the HTM (i.e., the formation of both amorphous and crystalline phases), which is an irreversible process.

In order to better understand whether tBP has a positive or negative impact on the HTM electronic properties, we performed four-probe measurements on spin-coated thin films (Figure S6) and found that aggregated crystalline SPIRO layers (aged HTM with tBP) were less conductive than amorphous SPIRO layers (fresh HTM with tBP), thus validating the ESR results and revealing the existence of a lower amount of defects in the SPIRO band gap and the induction of an irreversible de-doping process. This macroscopic evidence suggests that a crystalline SPIRO-based HTM (an aged, de-doped one) can be detrimental for the solar cell by negatively affecting the fill factor that is usually linked to the conductivity of the selective layers.

It is now required to unravel a chemical process though which $SPIRO^{+}$ molecules undergo the de-doping detected through ESR. Figure 5 shows the Raman spectra of different samples around 1,000 $cm^{-1}$. A distinct peak centered at 1,012 $cm^{-1}$ is visible in samples containing both $TFSI^{-}$ and tBP. This Raman peak was already attributed to pyridinium cation species.[29,30] The formation of a *tert*-butyl pyridinium cation ($tBP^{+}$), as a part of a pyridinated covalent adduct between $SPIRO^{+}$ molecules and tBP, was recently reported by Kasparavicius et al.[19] Therefore, a direct reaction of the tBP with the $SPIRO^{+}$ is responsible for a quenching of the radical in the material. In addition, one can expect that $TFSI^{-}$ acts as the counter-anion for $tBP^{+}$, as happens for well-known pyridinium-based ionic liquids.[31]

The formation of such $tBP^{+}$ species proceeds though a chemical mechanism that is described in Figure 5B. In this process, a one-electron reduction of $SPIRO^{+}$ molecules takes place by means of tBP molecules (which are present in large excess within the HTM mixture). This generates a de-doped SPIRO (neutral species) and a *tert*-butyl pyridinium radical cation, which is an unstable intermediate (in square brackets

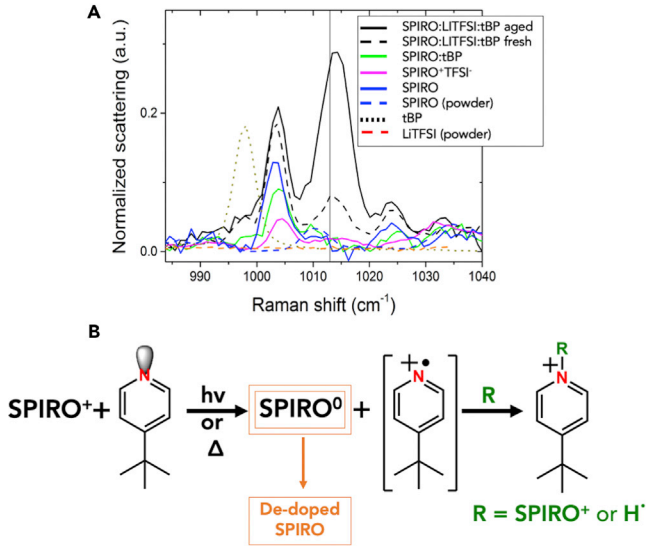


**Figure 5. De-doping Mechanism of SPIRO**

(A) Effect of tBP addition on a SPIRO-based HTM. Raman spectra show evidence of tBP formation at 1,012 $cm^{-1}$. "SPIRO (powder)" refers to the reagent-grade SPIRO material taken as a solid; the reference sample "$SPIRO^{+}TFSI^{-}$" was obtained by removing the solvent *in vacuo* from the solution of SPIRO:LiTFSI.

(B) Proposed mechanism for SPIRO de-doping in the presence of excess tBP.

in Figure 5B), and therefore, even if it is a radical, it is not detected through ESR. The pyridinium radical cation immediately reacts indeed with another $SPIRO^{+}$ molecule, leading to the pyridinated adduct between SPIRO and tBP previously reported in Kasparavicius et al.[19] Such an adduct is a charged species but does not contain unpaired electrons, and therefore, it is also invisible to ESR. In addition, since it contains a pyridinium cation within its molecular structure, it is responsible for the intense Raman signal that we detect at 1,012 $cm^{-1}$. Finally, the positive charge on the cationic species is compensated by the presence of $TFSI^{-}$ anions.

We also propose an alternative route for the formation of $tBP^{+}$ species (again in Figure 5B), which counts for the extraction of a hydrogen radical (H·) from a neutral tBP molecule by means of the tBP radical cation intermediate. The hydrogen radical is likely taken from the *tert*-butyl residues, and the process can take place reasonably because of the large excess in tBP present in the HTM mixture. The product of this radical reaction is again a pyridinium cation, bearing $TFSI^{-}$ as counter-anion, whose existence can again be related to the Raman signal at 1,012 $cm^{-1}$. The fate of the radicals generated after hydrogen extraction can then be multiple and difficult to unravel. A possible route can involve the pairing of two radicals to form a dimer, but other complex radical processes can also take place.

## Conclusions

In conclusion, in this work we have demonstrated an active role of tBP in SPIRO-based hole-transporting layers for PSC and that it impressively affects both the internal structural characteristic of this HTM and its electronic properties. In detail, the addition of tBP creates a semi-liquid environment in solid films that allows the structural reorganization of the SPIRO molecules, quickly rearranging from an amorphous state to a more crystalline structure. ESR and Raman analyses suggest that a

de-doping mechanism occurs within the HTM inducing such an irreversible reorganization of the molecules. Given that this is the first time that this mechanism has been proved, to the best of our knowledge, it goes against the general conception of SPIRO as an amorphous HTM, able to passivate perovskite interfacial defects. It further suggests that the great advantage of the SPIRO HTM production process (i.e., the use of high-boiling-point tBP) is limited to the morphological role of tBP, which permits solid-state diffusion of molecules with consequent pinhole passivation. However, tBP induces also a fast de-doping of the doped SPIRO HTM, by the chemical interaction with $SPIRO^+$ providing $tBP^+$ (as suggested by Kasparavicius et al.[19] and indicated here by our Raman data) $TFSI^-$ counter-anions, which have the major effect of reducing the overall conductivity of the SPIRO layer (proved by four-probe measurements). This could consequently affect the fill factor in a PSC.

Therefore, because SPIRO is a defect-mediated HTM, using a trap quencher such as tBP becomes a limiting factor for its performance in PSCs.

## EXPERIMENTAL PROCEDURES

### Sample Preparation

A standardized recipe[17] was used for preparing SPIRO solutions containing 56 mM SPIRO (Lumtec), 32 mM LiTFSI (Sigma Aldrich), and 195 mM *tert*-butylpyridine (tBP; Sigma Aldrich) in a dichlorobenzene-acetonitrile mixed solvent. All solvents were purchased from Sigma Aldrich. Several solutions were prepared: (1) fresh SPIRO only (labeled SPIRO sample), (2) fresh SPIRO with LiTFSI and tBP (labeled SPIRO:LiTFSI:tBP sample), (3) fresh SPIRO without LiTFSI with tBP (labeled SPIRO:tBP), (4) fresh SPIRO with LiTFSI without tBP (labeled SPIRO:LiTFSI sample), and (5) tBP only (labeled tBP sample). The solutions were prepared in a glovebox under a nitrogen atmosphere until used.

### ESR Measurements

All ESR measurements were performed on a Bruker ELEXSYS E580 spectrometer at X-band (9–10 GHz) mounting an ER4118X-MD5 dielectric cavity. Measurements were carried at 80 K, employing a liquid-$N_2$ cooling system. Continuous-wave spectra were typically acquired at 20–40 μW microwave power and 0.8 G field modulation amplitude. ESR measurements were conducted (1) in solution and air (some drops of the solution is put into an ESR quartz tube open in air) or (2) in film and vacuum (the solvent is evaporated out of the sample tube and the resulting solid film is left at the bottom and on the tube inner surface; the tube is then sealed under vacuum at $\sim 10^{-5}$ bar). ESR spectra were recorded in dark conditions or in light by exposing the sample to white light.

### Raman Measurements

Using an inVia Renishaw instrumentation, spectra were recorded to exploit as an excitation source a laser diode at 785 nm at a power of 1 $W/cm^2$. The system was calibrated against the 520.5 $cm^{-1}$ line of an internal silicon wafer. The spectra were registered in the 200–3,000 $cm^{-1}$ range. The final data were averaged over 100 accumulations in order to maximize the signal-to-noise ratio. The measurements were conducted at room temperature on a solid blend deposited into ESR tubes with the 5× objective.

## SUPPLEMENTAL INFORMATION

Supplemental Information can be found online at https://doi.org/10.1016/j.chempr.2019.04.003.

## ACKNOWLEDGMENTS

This work was financially supported by the OPERA project of "Centro Studi di Economia e Tecnica dell' Energia Giorgio Levi Cases" of the University of Padova.

## AUTHOR CONTRIBUTIONS

Conceptualization, F.L., E.C., T.G., and L.F.; Methodology, F.L., E.C., T.G., and A.R.; Validation, F.L., E.C., and R.S.; Investigation, F.L., E.C., T.G., and R.S.; Resources, M.M., A.P., and G.M.; Writing – Original Draft, F.L., T.G., and L.F.; Writing – Review & Editing, F.L., T.G., A.R., E.M., M.M., A.P., and L.F.; Supervision, F.L. and L.F.; Project Administration, E.M, G.M., M.M., and L.F.; Funding Acquisition, E.M., G.M., M.M., and L.F.

## DECLARATION OF INTERESTS

The authors declare no competing interests.

Received: January 18, 2019
Revised: March 18, 2019
Accepted: April 8, 2019
Published: May 2, 2019

## REFERENCES AND NOTES

1. Juarez-Perez, E.J., Leyden, M.R., Wang, S., Ono, L.K., Hawash, Z., and Qi, Y. (2016). Role of the dopants on the morphological and transport properties of spiro-MeOTAD hole transport layer. Chem. Mater. *28*, 5702–5709.

2. Ding, I.-K., Tétreault, N., Brillet, J., Hardin, B.E., Smith, E.H., Rosenthal, S.J., Sauvage, F., Grätzel, M., and McGehee, M.D. (2009). Pore-filling of spiro-OMeTAD in solid-state dye sensitized solar cells: quantification, mechanism, and consequences for device performance. Adv. Funct. Mater. *19*, 2431–2436.

3. Docampo, P., Hey, A., Guldin, S., Gunning, R., Steiner, U., and Snaith, H.J. (2012). Pore filling of spiro-OMeTAD in solid-state dye-sensitized solar cells determined via optical reflectometry. Adv. Funct. Mater. *22*, 5010–5019.

4. Kim, H.S., Lee, C.R., Im, J.H., Lee, K.B., Moehl, T., Marchioro, A., Moon, S.J., Humphry-Baker, R., Yum, J.H., Moser, J.E., et al. (2012). Lead iodide perovskite sensitized all-solid-state submicron thin film mesoscopic solar cell with efficiency exceeding 9%. Sci. Rep. *2*, 591.

5. Zhou, W., Wen, Z., and Gao, P. (2018). Less is more: dopant-free hole transporting materials for high-efficiency perovskite solar cells. Adv. Energy Mater. *8*, 1702512.

6. Gatti, T., Casaluci, S., Prato, M., Salerno, M., Di Stasio, F., Ansaldo, A., Menna, E., Di Carlo, A., and Bonaccorso, F. (2016). Boosting perovskite solar cells performance and stability through doping a poly-3(hexylthiophene) hole transporting material with organic functionalized carbon nanostructures. Adv. Funct. Mater. *26*, 7443–7453.

7. Gatti, T., Lamberti, F., Topolovsek, P., Abdu-Aguye, M., Sorrentino, R., Perino, L., Salerno, M., Girardi, L., Marega, C., Rizzi, G.A., et al. (2018). Interfacial morphology addresses performance of perovskite solar cells based on composite hole transporting materials of functionalized reduced graphene oxide and P3HT. Sol. RRL *2*, 1800013.

8. Arora, N., Dar, M.I., Hinderhofer, A., Pellet, N., Schreiber, F., Zakeeruddin, S.M., and Grätzel, M. (2017). Perovskite solar cells with CuSCN hole extraction layers yield stabilized efficiencies greater than 20%. Science *358*, 768–771.

9. Fantacci, S., De Angelis, F., Nazeeruddin, M.K., and Grätzel, M. (2011). Electronic and optical properties of the spiro-MeOTAD hole conductor in its neutral and oxidized forms: a DFT/TDDFT investigation. J. Phys. Chem. C *115*, 23126–23133.

10. Burschka, J., Pellet, N., Moon, S.J., Humphry-Baker, R., Gao, P., Nazeeruddin, M.K., and Grätzel, M. (2013). Sequential deposition as a route to high-performance perovskite-sensitized solar cells. Nature *499*, 316–319.

11. Namatame, M., Yabusaki, M., Watanabe, T., Ogomi, Y., Hayase, S., and Marumoto, K. (2017). Direct observation of dramatically enhanced hole formation in a perovskite-solar-cell material spiro-OMeTAD by Li-TFSI doping. Appl. Phys. Lett. *110*, 123904.

12. Shi, D., Qin, X., Li, Y., He, Y., Zhong, C., Pan, J., Dong, H., Xu, W., Li, T., Hu, W., et al. (2016). Spiro-OMeTAD single crystals: remarkably enhanced charge-carrier transport via mesoscale ordering. Sci. Adv. *2*, e1501491.

13. Abate, A., Hollman, D.J., Teuscher, J., Pathak, S., Avolio, R., D'Errico, G., Vitiello, G., Fantacci, S., and Snaith, H.J. (2013). Protic ionic liquids as p-dopant for organic hole transporting materials and their application in high efficiency hybrid solar cells. J. Am. Chem. Soc. *135*, 13538–13548.

14. Wang, S., Sina, M., Parikh, P., Uekert, T., Shahbazian, B., Devaraj, A., and Meng, Y.S. (2016). Role of 4- tert -butylpyridine as a hole transport layer morphological controller in perovskite solar cells. Nano Lett. *16*, 5594–5600.

15. Wang, S., Huang, Z., Wang, X., Li, Y., Günther, M., Valenzuela, S., Parikh, P., Cabreros, A., Xiong, W., and Meng, Y.S. (2018). Unveiling the role of tBP–LiTFSI complexes in perovskite solar cells. J. Am. Chem. Soc. *140*, 16720–16730.

16. Katoh, R., Kasuya, M., Furube, A., Fuke, N., Koide, N., and Han, L. (2009). Quantitative study of solvent effects on electron injection efficiency for black-dye-sensitized nanocrystalline TiO2 films. Sol. Energy Mater. Sol. Cells *93*, 698–703.

17. Tao, C., Van Der Velden, J., Cabau, L., Montcada, N.F., Neutzner, S., Srimath Kandada, A.R., Marras, S., Brambilla, L., Tommasini, M., Xu, W., et al. (2017). Fully solution-processed n-i-p-like perovskite solar cells with planar junction: how the charge extracting layer determines the open-circuit voltage. Adv. Mater. *29*, 1604493.

18. Magomedov, A., Kasparavičius, E., Rakstys, K., Paek, S., Gasilova, N., Genevičius, K., Juška, G., Malinauskas, T., Nazeeruddin, M.K., and Getautis, V. (2018). Pyridination of hole transporting material in perovskite solar cells questions the long-term stability. J. Mater. Chem. C *6*, 8874–8878.

19. Kasparavicius, E., Magomedov, A., Malinauskas, T., and Getautis, V. (2018). Long-term stability of the oxidized hole-transporting materials used in perovskite solar cells. Chemistry *24*, 9910–9918.

20. Tao, C., Neutzner, S., Colella, L., Marras, S., Srimath Kandada, A.R., Gandini, M., De Bastiani, M., Pace, G., Manna, L., Caironi, M.,

et al. (2015). 17.6% stabilized efficiency in low-temperature processed planar perovskite solar cells. Energy Environ. Sci. *8*, 2365–2370.

21. Lee, S.Y., and Boo, B.H. (1996). Density functional theory study of vibrational spectra of fluorene. J. Phys. Chem. *100*, 8782–8785.

22. Herstedt, M., Henderson, W.A., Smirnov, M., Ducasse, L., Servant, L., Talaga, D., and Lassègues, J.C. (2006). Conformational isomerism and phase transitions in tetraethylammonium bis(trifluoromethanesulfonyl)imide Et4NTFSI. J. Mol. Struct. *783*, 145–156.

23. Marczewski, M.J., Stanje, B., Hanzu, I., Wilkening, M., and Johansson, P. (2014). "Ionic liquids-in-salt" – a promising electrolyte concept for high-temperature lithium batteries? Phys. Chem. Chem. Phys. *16*, 12341–12349.

24. Brouillette, D., Irish, D.E., Taylor, N.J., Perron, G., Odziemkowski, M., and Desnoyers, J.E. (2002). Stable solvates in solution of lithium bis(trifluoromethylsulfone)imide in glymes and other aprotic solvents: phase diagrams, crystallography and Raman spectroscopy. Phys. Chem. Chem. Phys. *4*, 6063–6071.

25. Hawash, Z., Ono, L.K., and Qi, Y. (2018). Recent advances in spiro-MeOTAD hole transport material and its applications in organic-inorganic halide perovskite solar cells. Adv. Mater. Interfaces *5*, 1700623.

26. Hardwick, L.J., Holzapfel, M., Wokaun, A., and Novák, P. (2007). Raman study of lithium coordination in EMI-TFSI additive systems as lithium-ion battery ionic liquid electrolytes. J. Raman Spectrosc. *38*, 110–112.

27. Blackmore, I.J., Gibson, V.C., Hitchcock, P.B., Rees, C.W., Williams, D.J., and White, A.J.P. (2005). Pyridine N-alkylation by lithium, magnesium, and zinc alkyl reagents: synthetic, structural, and mechanistic studies on the bis(imino)pyridine system. J. Am. Chem. Soc. *127*, 6012–6020.

28. Petty, M.C. (2007). Organic and Molecular Electronics: From Principles to Practice, First ed. (John Wiley & Sons, Ltd).

29. Rogers, D.J., Luck, S.D., Irish, D.E., Guzonas, D.A., and Atkinson, G.F. (1984). Surface enhanced Raman spectroscopy of pyridine, pyridinium ions and chloride ions adsorbed on the silver electrode. J. Electroanal. Chem. Interfacial Electrochem. *167*, 237–249.

30. Regis, A., and Corset, J. (1980). A chemical interpretation of the intense Raman spectra observed at a silver electrode in the presence of chloride ion and pyridine: Formation of radicals. Chem. Phys. Lett. *70*, 305–310.

31. Chaban, V.V., and Prezhdo, O.V. (2016). Ionic vapor composition in pyridinium-based ionic liquids. J. Phys. Chem. B *120*, 4661–4667.